

Correlation of Vibrational and Electronic Spectra. 1. Vibronic Intensity Distributions and Ligand-Field Strengths in d–d Spectra of Five Planar CuCl₂X₂ Chromophores

Adam J. Bridgeman, Sarah J. Essex, and Malcolm Gerloch*

University Chemical Laboratories, Cambridge University, Lensfield Road, Cambridge CB2 1EW, UK

Received November 5, 1993[⊗]

A new approach is presented for the modeling of vibronic intensities of centrosymmetric transition metal “d–d” spectra. Relative contributions to intensity from different vibrational modes are determined by prior normal coordinate analysis of the vibrational spectra. The remaining variables in this cellular ligand-field (CLF) approach then relate to electronic, bonding factors alone as in our earlier model for acentric chromophores. The intensity distributions in five centric, planar chromophores, three with CuCl₂N₂ coordination and two with CuCl₂O₂, have been reproduced quantitatively by this new model. The vibronic intensity analyses are predicated upon CLF analysis of transition energies. The combination of energy and intensity analyses in these studies has removed earlier assignment ambiguities that could not be resolved by energy analyses and symmetry alone. An important feature of the CLF energy analyses of the CuCl₂N₂ species has been the establishment of large ligand-field strengths for ligations with heterocyclic imines, together with unusually large values of the associated ligand-field trace. These are ascribed to a significant ligand polarity within the complex, an interpretation which has wider implications for the understanding of CLF energy parameters in general. All CLF intensity parameter values appear to be consistent with this view and with those previously established from analyses of a wide range of acentric chromophores.

Introduction

Ligand-field studies of the “d–d” spectra of transition metal complexes usually focuses exclusively upon transition energies. Their modeling within the cellular ligand-field (CLF) approach has been quite generally successful.^{1,2} The e_{λ} parameters of that scheme reflect the spatial and functional superposition inherent in a modeling designed to provide meaningful chemical commentary upon the character of metal–ligand bonding. Somewhat recent extensions^{3–5} of the approach have addressed the intensities of “d–d” transitions. Electric dipole intensity arises through the admixture of small amounts of odd parity functions into the d basis. Those functions derive from the bonding orbitals in any given complex and, hence, largely from the ligand valence orbitals. Transition moments are parameterized with t_{λ} variables which, like the e_{λ} energy parameters above, probe the local nature of the electron distribution within the underlying metal–ligand bonds.

Our first intensity model was applicable only to acentric chromophores wherein parity mixing arises from the equilibrium environment: we refer to this approach as the *static* model.³ Recently, we have published a development⁶ of this scheme designed specifically to address those very many centric chromophores in which the necessary parity mixing arises dynamically during the course of *ungerade* molecular vibrations. This *vibronic* or *dynamic* model is parameterized with the variables $t_{\lambda}^{\alpha}(Q)$ in which α refers to the direction of a ligand

displacement within the normal mode Q . This new approach has quantitatively reproduced the polarized “d–d” spectra of several planar tetrahalcocopper(II) and -platinum(II) chromophores.^{7,8} Though successful, those analyses were technically difficult in view of the high degree of parameterization that is necessarily associated with a free accounting of several dynamically independent vibrations. For the copper species, for example, several fits to the experimental data were discovered in significantly different regions of parameter space.

Theoretically, however, the new vibronic model⁶ formally relates t_{λ}^{α} parameters referring to different vibrational modes to underlying, static-type t_{λ} parameters and to the amplitudes of the normal modes. The latter may be derived from a proper analysis of the experimental vibrational frequencies of the object chromophore. After such a process, the intensity t parameters for a dynamically sourced chromophore are of precisely the same kind as those for a statically sourced system and so analyses for centric and acentric species proceed on the same footing. The t parameters then relate exclusively to electronic features of the chemical bonding.

The current modeling, incorporated within the software of our program suite,⁹ CAMMAG4, is thus applicable with equal facility to acentric and centric chromophores and to those near-centric species in which intensity is expected to arise from *both* static and dynamic sources. In the following paper,¹⁰ we report on an analysis of the “d–d” dipole and rotatory strengths in the tris(ethylenediamine)nickel(II) ion. That and the present paper, therefore, are the first to describe analyses in which the mechanical and electronic aspects of “d–d” electronic spectra are separated in this way.

The completed vibronic model is described and applied here to the polarized spectra of two, planar *trans* CuCl₂O₂ and three

[⊗] Abstract published in *Advance ACS Abstracts*, October 15, 1994.

- (1) Gerloch, M. *Magnetism & Ligand-Field Analysis*, Cambridge University Press: Cambridge, UK, 1983.
- (2) Duer, M. J.; Fenton, N. D.; Gerloch, M. *Int. Rev. Phys. Chem.* **1990**, *9*, 227.
- (3) Brown, C. A.; Gerloch, M.; McMeeking, R. F. *Mol. Phys.* **1988**, *64*, 771.
- (4) Brown, C. A.; Duer, M. J.; Gerloch, M.; McMeeking, R. F. *Mol. Phys.* **1988**, *64*, 793.
- (5) Brown, C. A.; Duer, M. J.; Gerloch, M.; McMeeking, R. F. *Mol. Phys.* **1988**, *64*, 825.
- (6) Duer, M. J.; Essex, S. J.; Gerloch, M.; Jupp, K. M. *Mol. Phys.* **1993**, *79*, 1147.

- (7) Duer, M. J.; Essex, S. J.; Gerloch, M. *Mol. Phys.* **1993**, *79*, 1167.
- (8) Bridgeman, A. J.; Gerloch, M. *Mol. Phys.* **1993**, *79*, 1195.
- (9) Dale, A. R.; Duer, M. J.; Fenton, N. D.; Gerloch, M.; McMeeking, R. F. CAMMAG4, a FORTRAN computer program, 1991.
- (10) Bridgeman, A. J.; Jupp, K. M.; Gerloch, M. *Inorg. Chem.*, following paper in this issue.

Table 1. Chromophores Studied in This Work^a

abbrevn	compound	coordination	IR/Raman	normal coord anal.	polarized d-d spectra	AOM anal.
PDMP	Cu(1-phenyl-3,5-dimethylpyrazole) ₂ Cl ₂	CuCl ₂ N ₂	12, 13		12, 13	13
2,3-LUT	Cu(2,3-dimethylpyridine) ₂ Cl ₂	CuCl ₂ N ₂	12, 13		12, 13	13
2,6-LUT	Cu(2,6-dimethylpyridine) ₂ Cl ₂	CuCl ₂ N ₂	12, 13	13	12, 13	13
4-PICNO	Cu(4-methylpyridine- <i>N</i> -oxide) ₂ Cl ₂	CuCl ₂ O ₂	11, 13		11, 13	13
DIAQ	Cu(H ₂ O) ₂ Cl ₂ ·4(C ₆ H ₅) ₃ PO	CuCl ₂ O ₂	11, 13	13	11, 13	13

^a The last four columns cite other work by reference number.

similar CuCl₂N₂ chromophores. Hitchman and McDonald^{11–13} have published careful and extensive studies of both vibrational and electronic spectra of these molecules, together with some vibrational and angular overlap model (AOM) analyses. Table 1 lists names and abbreviations for these five systems and summarizes our data base. The “d–d” intensity analyses have proceeded smoothly in all cases. For each of the five chromophores, we have been able to reproduce relative “d–d” transition intensities and to account quantitatively for the temperature variation of the “d–d” transition intensities, essentially within experimental error. The successful completion of these intensity analyses rests in part upon preceding energy analyses. At the same time, ambiguities in some of the energy studies are removed by the intensity work. Some important conclusions about the energy parameters and ligand-field traces emerge from these analyses, conclusions that are supported by the intensity parameters determined subsequently.

Transition Energies

CuCl₂N₂ Species. Crystal structure analyses have been reported^{14–16} for each of the PDMP, 2,3-LUT, and 2,6-LUT species. The CuCl₂N₂ chromophoric moieties all closely approximate *D*_{2h} symmetry, as sketched in Figure 1, and the heterocycles lie in planes that are nearly normal to the CuCl₂N₂ plane in each molecule. The full CLF parameter set comprises the following: *e*_σ(Cl) and *e*_π(Cl) for σ and π Cu–Cl interaction; *e*_σ(N) and *e*_{π⊥}(N) for Cu–heterocyclic bonding (⊥ means normal to the local heterocycle) with *e*_{π||} = 0; and *e*_σ(void) for the ligand field of a coordination void.^{17,18}

In the limit of *D*_{2h} coordination geometry, and with the neglect of spin–orbit coupling, relative orbital energies in these species are given by¹⁹

$$\begin{aligned} \epsilon(x^2-y^2) &= 3/2[e_\sigma(\text{Cl}) + e_\sigma(\text{N})] \\ \epsilon(xy) &= 2e_\pi(\text{Cl}) + 2e_{\pi_\perp}(\text{N}) \\ \epsilon(xz) &= 0 \\ \epsilon(yz) &= 2e_\pi(\text{Cl}) \\ \epsilon(z^2) &= 1/2[e_\sigma(\text{Cl}) + e_\sigma(\text{N})] + 2e_\sigma(\text{void}) \end{aligned} \quad (1)$$

where *x* is taken parallel to Cu–N, *y* parallel to Cu–Cl, and *z* normal to the coordination plane. An off-diagonal term

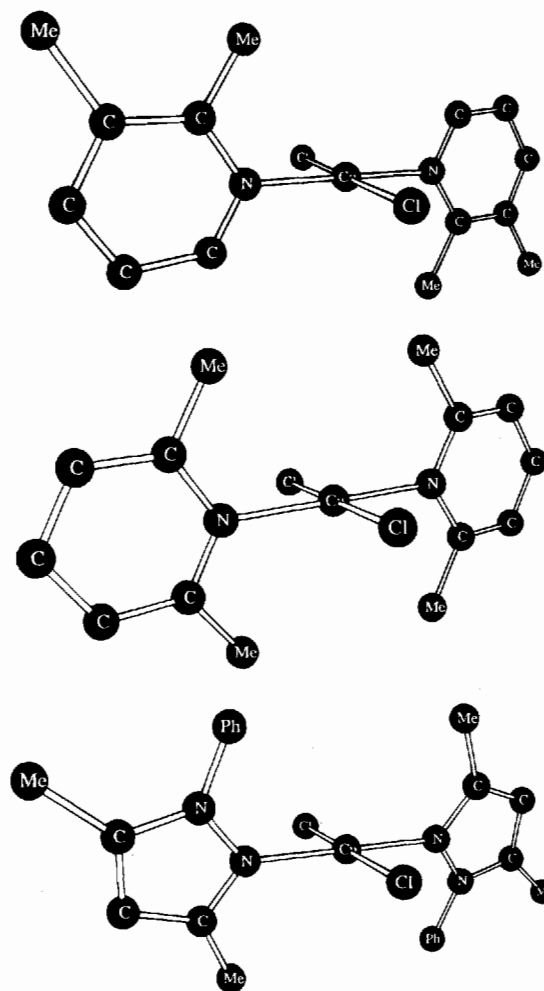


Figure 1. Molecular geometries of the CuCl₂N₂ species: (a, top) 2,3-LUT, (b, middle) 2,6-LUT, and (c, bottom) PDMP.

$\langle d_{z^2} | V_{LF} | d_{x^2-y^2} \rangle = 3^{1/2}[e_\sigma(\text{N}) - e_\sigma(\text{Cl})]/2$ also couples the *d*_{z²} and *d*_{x²-y²} functions in *D*_{2h} symmetry. Were it not for this coupling term, *e*_σ(N) and *e*_σ(Cl) values would be unresolvable as otherwise they consistently appear merely as their sum. Hence, to the extent that the difference [*e*_σ(N) – *e*_σ(Cl)] is small compared with the sum [*e*_σ(N) + *e*_σ(Cl)], we would expect to determine only the average values $\bar{e}_\sigma = [e_\sigma(\text{Cl}) + e_\sigma(\text{N})]/2$. In searching parameter space for a fit to experiment, therefore, we anticipate an extended region of correlation between optimal values of *e*_σ(N) and *e*_σ(Cl). Selected features of the first coordination shells are included in Table 2.

Accordingly, energy calculations have been performed within the complete *d*⁹ basis using the CLF variables, *e*_σ(N), *e*_σ(Cl), *e*_σ(void), *e*_π(Cl), and *e*_{π⊥}(N), together with the spin–orbit coupling parameter ζ . This latter was held fixed at 700 cm^{–1} after several checks of both energies and intensities were found to be incapable of resolving ζ to better than ± 200 cm^{–1} of this value. Analyses set up in this way proceeded smoothly but for the question of band assignment for the two highest transitions. Hitchman and McDonald^{12,13} favored $z^2 \rightarrow x^2 - y^2$ and

- (11) Hitchman, M. A.; McDonald, R. G. *Inorg. Chem.* **1990**, *29*, 3081.
- (12) Hitchman, M. A.; McDonald, R. G. *Inorg. Chem.* **1990**, *29*, 3074.
- (13) R. G. McDonald, Ph.D. Thesis, University of Tasmania, Hobart, Australia, 1988.
- (14) Francisco, R. H. P.; Lechat, J. R.; Massabui, A. C.; Melios, C. B.; Molina, M. *J. Coord. Chem.* **1980**, *10*, 149.
- (15) Stahlin, W.; Oswald, H. R. *Acta Crystallogr.* **1971**, *B27*, 1368.
- (16) Campbell, J. A.; Raston, C. L.; Varghese, J. N.; White, A. H. *Aust. J. Chem.* **1977**, *30*, 1947.
- (17) Deeth, R. J.; Gerloch, M. *Inorg. Chem.* **1984**, *23*, 3846.
- (18) Gerloch, M.; Harding, J. H.; Woolley, R. G. *Struct. Bonding* **1981**, *46*, 1.
- (19) Gerloch, M.; Slade, R. C. *Ligand-Field Parameters*; Cambridge University Press: Cambridge, UK, 1973.

Table 2. Structural Summary for CuCl_2N_2 Species

	PDMP	2,3-LUT	2,6-LUT
crystal class	monoclinic	monoclinic	triclinic
space group	$P2_1/c$	$P2_1/c$	$P1$
struct ref	14	15	16
Cu-Cl bond length/Å	2.27	2.25	2.26
Cu-N bond length/Å	1.98	1.98	2.01
Cl-Cu-N angle/deg	89.2, 90.8	89.4, 90.6	89.4, 90.6
dihedral angle between plane of heterocycle and CuCl_2N_2 /deg	79.8	88.4	86.4

Table 3. Optimal CLF Energy Parameter Values (cm^{-1}) for CuCl_2N_2 Chromophores^a

	PDMP	2,3-LUT	2,6-LUT
\bar{e}_σ	6550	6550	6350
$e_\pi(\text{Cl})$	1800	1280	1280
$e_{\pi\perp}(\text{N})$	950	940	940
$e_\sigma(\text{void})$	-2500	-2690	-2690
Σ	30300	27820	27020

^a Values for $e_\sigma(\text{N})$ and $e_\sigma(\text{Cl})$ are strongly correlated (see text) and such that, for PDMP, $e_\sigma(\text{N}) = -e_\sigma(\text{Cl}) + 13\,100$ in the range $e_\sigma(\text{Cl})$ 4000–7500; for 2,3-LUT, $e_\sigma(\text{N}) = -0.795e_\sigma(\text{Cl}) + 12\,000$ in the range 3500–6500; and for 2,6-LUT, $e_\sigma(\text{N}) = -0.85e_\sigma(\text{Cl}) + 11\,880$ in the range 3500–7500.

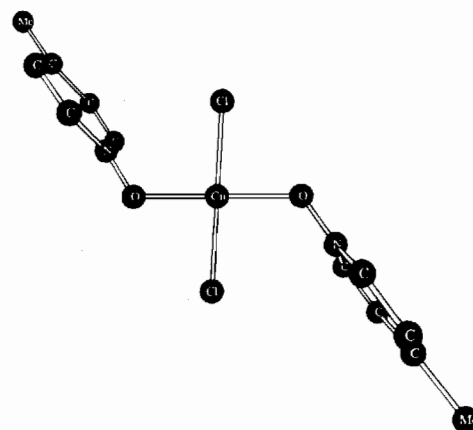
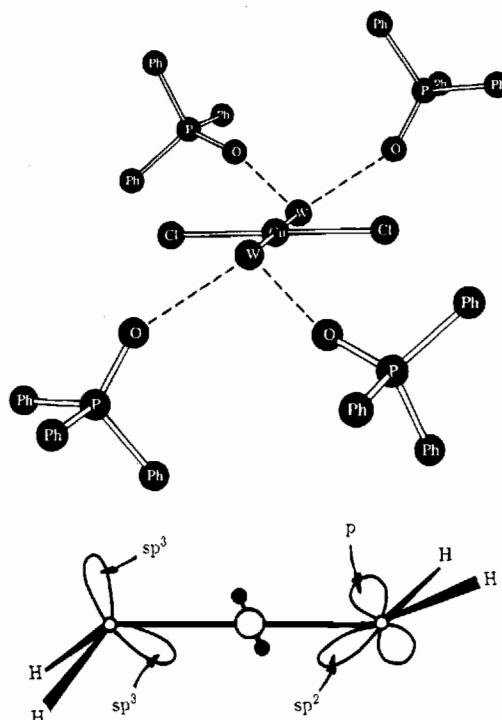
Table 4. Observed Transition Energies (cm^{-1}) in CuCl_2N_2 Species Compared with Those Calculated by Using the Optimal Parameter Values in Table 3

${}^2A_g(x^2-y^2) \rightarrow$	PDMP		2,3-LUT		2,6-LUT		band
	obsd	calcd	obsd	calcd	obsd	calcd	
${}^2B_{1g}(xy)$	14 100	14 116	15 400	15 168	14 700	14 571	1
${}^2B_{3g}(yz)$	16 100	16 004	17 280	16 981	16 600	16 405	2
${}^2A_g(z^2)$	17 800	18 002	18 600	18 407	18 000	18 928	3
${}^2B_{2g}(xz)$	20 000	19 711	20 600	20 037	19 800	19 431	4

$xz \rightarrow x^2 - y^2$, some 2000 cm^{-1} apart in each chromophore, as the highest and second-highest bands, respectively. They considered the reversed assignment of these two excitations to be possible also. We have examined both assignments in detail.

Excellent reproduction of all transition energies is possible for the favored assignment for an essentially unique set of CLF parameter values. The subsequent intensity analyses, however, were all quite unable to reproduce the observed intensity distributions. In each case, the failure was characterized by a strong tendency toward reversed relative intensities for the $z^2 \rightarrow x^2 - y^2$ and $xz \rightarrow x^2 - y^2$ transitions. Conversely, no problem arose with a reversed assignment of these transitions. Table 3 lists optimal CLF parameter values affording good reproduction of all transition energies with this alternative assignment. The correlation between $e_\sigma(\text{N})$ and $e_\sigma(\text{Cl})$ for optimal fit is given at footnote *a* of Table 3. The wide bounds preclude any confidence in individual values for these parameters. Accordingly, we quote the mean value, \bar{e}_σ , which was found to be essentially constant throughout the correlation. The quality of fit is shown in Table 4. Eigenvalues and eigenvectors produced with these optimal parameter sets were employed throughout the ensuing intensity analyses.

CuCl_2O_2 Species. Crystal structure analyses for both 4-PICNO and DIAQ have been reported.^{20,21} The molecular structure of 4-PICNO is shown in Figure 2 while Figure 3 illustrates details of both crystal and molecular structures of the DIAQ system. Salient dimensions are presented in Table 5. Again, the molecular geometries of each chromophore are

**Figure 2.** Molecular structure of 4-PICNO.**Figure 3.** (a, top) Probable hydrogen-bonding network in the crystal structure of DIAQ. (b, bottom) Limiting donor oxygen orbitals offered to the copper atom in DIAQ.**Table 5.** Structural Summary for CuCl_2O_2 Species

	DIAQ	4-PICNO
crystal class	monoclinic	monoclinic
space group	$P2_1/c$	$P2_1/c$
struct ref	21	20
Cu-Cl bond length/Å	2.24	2.23
Cu-O bond length/Å	1.90	1.95
Cl-Cu-O angle/deg	89.1, 90.9	86.4, 93.6

rigorously centric and of approximate D_{2h} symmetry. As usual, however, no idealizations of the molecular symmetry are employed in our CLF analyses (for energy or intensity), which were performed within the full d^9 configuration using reported crystallographic coordinates throughout.

The analyses for the CuCl_2O_2 species differ from those for the CuCl_2N_2 species in that the effects of misdirected valency² are to be recognized for the oxygen donors. Furthermore, the experimental data base is less good for the oxygen ligands, there being only three resolvable transition energies as opposed to four for the nitrogen ligands. As for the nitrogen species, we are unable to resolve $e_\sigma(\text{Cl})$ from $e_\sigma(\text{O})$ and refer henceforth to

(20) Johnson, D. R.; Watson, W. H. *Inorg. Chem.* **1971**, *10*, 1068.

(21) Dunaj-Jurco, M.; Kozisck, J.; Aneyskina, A.; Ondrejovic, G.; Makanova, D.; Gazo, J. *J. Chem. Soc., Chem. Commun.* **1979**, 654.

Table 6. Observed Transition Energies (cm⁻¹) in CuCl₂O₂ Species Compared with Those Calculated by Using the Optimal Parameter Values in Table 7

² A _g (x ² -y ²) →	DIAQ		² A _g (x ² -y ²) →	4-PICNO		band
	obsd	calcd		obsd	calcd	
² B _{2g} (xz)	13 300	13 329	² B _{1g} (xy)	12 750	12 757	1
² B _{3g} (yz)	15 200	14 831	² B _{3g} (yz)	14 500	14 516	2
² B _{1g} (xy)		15 469	² B _{2g} (xz)		14 762	
² A _g (z ²)	17 900	17 915	² A _g (z ²)	17 500	17 502	3

$\bar{e}_\sigma = 1/2[e_\sigma(\text{Cl}) + e_\sigma(\text{O})]$. For each CuCl₂O₂ chromophore, we include $e_\sigma(\text{void})$ and $\zeta = 700$ cm⁻¹ as system variables. The analyses for 4-PICNO and DIAQ require separate discussion with respect to the misdirected valency.

As shown in Figure 2, the planes of the picoline ligands lie at right angles to the CuCl₂O₂ coordination plane. The ligand-field consequence of the nonbonding oxygen lone pair of electrons is to render the local submatrix of d_{z^2} and d_{xz} orbitals nondiagonal. An off-diagonal CLF parameter $e_{\sigma\pi x}$ ($=e_{\sigma\pi l}$), together with a nonzero value for $e_{\pi x}$ ($e_{\pi l}$) and modified value for e_σ , account for this misdirected valency. Some degree of Cu-O π interaction in the plane normal to the ligand is to be expected also. The full CLF parameter set is thus \bar{e}_σ , $e_\pi(\text{Cl})$, $e_{\pi\perp}(\text{O})$, $e_{\sigma\pi l}$, $e_{\pi l}(\text{O})$, and $e_\sigma(\text{void})$ plus ζ as usual. So free a parameterization is clearly unsupportable with just three transition energies. Accordingly, we have reduced the degree of parameterization as follows. We set $e_{\sigma\pi l}(\text{O}) = +700$ cm⁻¹, the sign being determined by established conventions² and the magnitude being an estimate that should at least be better than a complete neglect of the misdirected valence effect.² In addition we set $e_{\pi l}(\text{O}) = e_{\pi\perp}(\text{O}) = e_\pi(\text{Cl})$. Though not ideal, the consequences of any errors here are likely to be relatively gentle upon ensuing values of \bar{e}_σ and $e_\sigma(\text{void})$. Together with $\zeta = 700$ cm⁻¹ again, there thus remain \bar{e}_σ , $e_\sigma(\text{void})$, and e_π to be determined by fitting to three observable transition energies.

The orbital transition energies, assuming the foregoing relationships together with ideal D_{2h} symmetry and no spin-orbit coupling, are given by

$$\begin{aligned}
 xy \rightarrow x^2 - y^2 & \quad 3e_\sigma - 4e_\pi + \epsilon \\
 xz \rightarrow x^2 - y^2 & \quad 3e_\sigma - 2e_\pi + \epsilon \\
 yz \rightarrow x^2 - y^2 & \quad 3e_\sigma - 2e_\pi + \epsilon \\
 z^2 \rightarrow x^2 - y^2 & \quad 2e_\sigma - 2e_\sigma(\text{void}) + 2\epsilon \quad (2)
 \end{aligned}$$

where ϵ is a function of the difference [$e_\sigma(\text{N}) - e_\sigma(\text{Cl})$]. Hitchman and McDonald^{11,13} have argued for a spectral assignment of 4-PICNO with transition energies increasing in the same order as in (2), the middle band being a composite of the $xz \rightarrow x^2 - y^2$ and $yz \rightarrow x^2 - y^2$ transitions. Our CLF energy analysis has proceeded on this basis. We have been able to reproduce all three transitions well, as shown in Table 6, with the, essentially unique, parameter values listed in Table 7.

The possibility for misdirected valence, either from the influence of a nonbonding lone pair, a misdirected donor hybrid orbital, or both, arises from the water ligands in the DIAQ system. Though not located by the crystal structure analysis,²¹ the water hydrogen atoms are likely to be hydrogen bonded to the lattice phosphine oxide molecules, as indicated in Figure 3a. The plane O(phosphine oxide)-O(water)-O(phosphine oxide) makes an angle of 34° to the CuCl₂O₂ coordination plane in such a way that the line of intersection of the two planes is nearly perpendicular to the Cu-O vector. If the hydrogen atoms

Table 7. Optimal CLF Energy Parameters (cm⁻¹) for CuCl₂O₂ Chromophores^a

	DIAQ		4-PICNO	
\bar{e}_σ	5700	\bar{e}_σ	5450	
$e_\pi(\text{Cl})$	1000	e_π	830	
$e_{\pi\perp}(\text{O})$	1800			
$e_{\pi l}(\text{O})$	0 ^b			
$e_{\sigma\pi l}(\text{O})$	0 ^b	$e_{\sigma\pi l}(\text{O})$	700	
$e_\sigma(\text{void})$	-3110 ^c	$e_\sigma(\text{void})$	-3110	
Σ	24180	Σ	22220	

^a Values for $e_\sigma(\text{O})$ and $e_\sigma(\text{Cl})$ are strongly correlated (see text) and such that, for DIAQ, $e_\sigma(\text{O}) = -0.966e_\sigma(\text{Cl}) + 11\,000$ in the range $e_\sigma(\text{Cl})$ 4500-6500, and for 4-PICNO, $e_\sigma(\text{O}) = -0.97e_\sigma(\text{Cl}) + 10435$ in the range 4000-6500. ^b Fixed. ^c Set Equal to $e_\sigma(\text{void})$ for 4-PICNO.

lie in, or close to, the O-O-O plane, orbitals offered to the metal atom for bonding by the water oxygen will lie close to the plane normal to the CuCl₂O₂ moiety. If the water oxygen is formally sp² hybridized, the oxygen donor orbitals are an sp² hybrid and a "pure" p function, as shown on one water ligand in figure 3b: if sp³ hybridized, a pair of sp³ hybrids lie in the plane normal to CuCl₂O₂, as indicated on the other water ligand in Figure 3b. In either case, or indeed for any circumstance in between these limits, a proper CLF parameterization of the Cu-water interaction would include $e_\sigma(\text{O})$, $e_{\pi\perp}(\text{O})$, and $e_{\sigma\pi l}(\text{O})$ variables with $e_{\pi l}(\text{O}) = 0$, where \parallel and \perp refer to the CuCl₂O₂ coordination plane.

As before, we cannot distinguish $e_\sigma(\text{O})$ and $e_\sigma(\text{Cl})$. Also, only three transition energies can be resolved experimentally. So we have simplified our CLF analyses by taking the following variable set: \bar{e}_σ , $e_\pi(\text{Cl})$, and $e_{\pi\perp}(\text{O})$, with $e_{\sigma\pi l}(\text{O}) = 0$ and $e_\sigma(\text{void})$ equal to that value determined for the 4-PICNO complex; $\zeta = 700$ cm⁻¹ as usual. The choice of $e_{\sigma\pi l}(\text{O}) = 0$ is less arbitrary than might appear. To a considerable extent (to the extent, in fact, of ignoring spin-orbit coupling) the d_{xz} orbital is affected only by $e_{\pi\perp}(\text{O})$ and $e_{\sigma\pi l}(\text{O})$. An incorrect, fixed value for $e_{\sigma\pi l}$ will be adjusted for by small changes in $e_\sigma(\text{O})$ (and hence in \bar{e}_σ) and by larger changes in $e_{\pi\perp}$. So these values may be in error but the final energies and wavefunctions should be substantially correct. The intensity analyses are predicated on these rather than upon the parameterization scheme that produced them.

Orbital transition energies, corresponding to (2), derived without spin-orbit coupling but with ideal D_{2h} chromophore symmetry together with the relationships above are

$$\begin{aligned}
 xy \rightarrow x^2 - y^2 & \quad 3\bar{e}_\sigma - 2e_\pi(\text{Cl}) + \epsilon \\
 xz \rightarrow x^2 - y^2 & \quad 3\bar{e}_\sigma - 2e_{\pi\perp}(\text{O}) + \epsilon \\
 yz \rightarrow x^2 - y^2 & \quad 3\bar{e}_\sigma - 2e_\pi(\text{Cl}) + \epsilon \\
 z^2 \rightarrow x^2 - y^2 & \quad 2\bar{e}_\sigma - 2e_\sigma(\text{void}) + 2\epsilon \quad (3)
 \end{aligned}$$

with ϵ defined as below (2). It follows that the transitions $xy \rightarrow x^2 - y^2$ and $yz \rightarrow x^2 - y^2$ are degenerate within these approximations and that they are within the middle energy band if $e_\pi(\text{Cl}) < e_{\pi\perp}(\text{O})$ or within the lowest band if $e_\pi(\text{Cl}) > e_{\pi\perp}(\text{O})$. Hitchman and McDonald,^{11,13} however, have assigned the bands in the ascending energy order $xy \rightarrow$, $(xy, yz) \rightarrow$, and $z^2 \rightarrow$ on the apparently unambiguous grounds that the weakest transition observed in any polarization is for the light dipole oriented normal to the CuCl₂O₂ plane for the lowest energy transition and that transition is forbidden, group theoretically. If $e_\pi(\text{Cl}) < e_{\pi\perp}(\text{O})$, this very weak transition is assigned as $xz \rightarrow x^2 - y^2$, which is vibronically allowed for a b_{3u} mode. Our disagreement with Hitchman and McDonald rests, of course,

upon our assumption that the water hydrogens are involved in hydrogen bonding with the phosphine oxides of the lattice, essentially in the O—O—O planes.

We have accordingly completed our CLF energy analysis within the preceding basis. Excellent reproduction of the transition energies, as shown in Table 6, has been achieved with the parameter set in Table 7. The subsequent intensity analysis has proved entirely successful, and the reasons for assignment problems will be clarified later. Intensity analyses predicated on the assumption that $e_{\pi}(\text{Cl}) > e_{\pi}(\text{O})$ were unsuccessful.

Transition Intensities

Review of the Theoretical Model. The static³ and dynamic⁶ CLF intensity models have been published in full. The present brief review emphasizes, so far as possible, their nonmathematical aspects but also serves to define properly the advance made by the present series of studies upon these primary approaches.

Two main features characterize, and are responsible for the success of, the CLF energy model.¹ It is a ligand-field model, employing a mean effective one-electron operator acting within a pure d (or f) basis and it exploits a principle of spatial (or cellular) superposition, so providing the link with chemical functionality that is so necessary. These same features are incorporated into the CLF intensity models. The cellular decomposition obliges us to define quantities with respect to both global (molecular) and local (ligation) reference frames. Electric dipole intensity is proportional to the squares of appropriate transition moments, \mathbf{M} (or to $\mathbf{M}^*\mathbf{M}$, where \mathbf{M} is complex). Experimental transitions relate directly to global transition moments between states Ψ_i and Ψ_j :

$$\mathbf{M} = \langle \Psi_i | e\mathbf{r} | \Psi_j \rangle \quad (4)$$

The electric dipole operator $e\mathbf{r}$ is a vector operator, with three components necessary to describe the orientation of the oscillating light dipole with respect to the global frame. Therefore, \mathbf{M} similarly has three such components; experimentally these refer to the familiar polarized spectra obtained in single crystal experiments. Adoption of the cellular structure of the model implies the assumption that electronic transitions involve only local movements of electron density; several simultaneous local displacements throughout the molecule are envisaged, of course. Our CLF models effectively incorporate a cellular factorization of the kind

$$\mathbf{M}_{\text{global}} = \sum_{\text{cells}} \mathbf{M}_{\text{local}} \quad (5)$$

so we next enquire about local transition moments:

$$\mathbf{M}_{\text{local}} = \langle \phi_i^{\text{LFO}} | e\mathbf{r} | \phi_j^{\text{LFO}} \rangle \quad (6)$$

when ϕ^{LFO} means a local ligand-field orbital as defined in ref 1. Exploitation of the *ligand-field* ansatz then asks for the construction of operator equivalents such that the local transition moments are expressed as integrals within the pure d (or f) basis, as usual:

$$\mathbf{M}_{\text{local}} = \langle \phi_i | e\mathbf{r} | \phi_j \rangle \equiv \langle d_i | e\mathbf{T} | d_j \rangle \quad (7)$$

For nonvanishing \mathbf{M} , the operators $e\mathbf{T}$ must include parts of even parity. These arise from the combination of the odd-parity dipole operator $e\mathbf{r}$ together with any odd-parity parts of the LFOs, ϕ . Thus intensity arises through parity mixing into the d basis. Empirically, “d—d” transitions are weak and so we

know that the LFOs are dominated by d character; all this is part and parcel of the ligand-field “regime”.

The integrals in (7) are rather similar to those one-electron integrals involved in CLF energy theory:

for energies

$$\langle d_i | v_{\text{LF}} | d_j \rangle \text{ parameterized by the } \{e_{\lambda}\}$$

for transition moments

$$\langle d_i | e\mathbf{T} | d_j \rangle \text{ parameterized by the } \{L_{t\lambda}\}$$

Using standard techniques of angular momentum theory (most conveniently, by tensor operator theory), local quantities are transformed into (or referred to) the global frame and summed. For energies, this means that global (G) ligand-field matrix elements, $\langle d_i | V_{\text{LF}}^G | d_j \rangle$, are ultimately expressed as (geometry defined) sums of local e_{λ} . For intensities, global transition moments, $\langle d_i | e\mathbf{T}^G | d_j \rangle$, are similarly expressed as sums of the local $L_{t\lambda}$ parameters. The local e_{λ} are energies; the local $L_{t\lambda}$ are transition moments.

The subscript λ ($\equiv \sigma, \pi_x, \pi_y$) labels the further functional subdivision of the superposition that so transparently relates to chemistry and bonding. The t parameters, however, bear a further label, the left superscript L . L takes the value P or F , for the most part, and so we have a double layer of intensity parameterization— $P_{t\lambda}$ and $F_{t\lambda}$. This complication—which actually yields a useful bonding metric not offered by the energy parameterization—arises as follows.

The LFOs are built essentially from the (dominant) d orbital and a local bonding orbital. This latter will generally be dominated by ligand valence orbitals but will include metal s and a little p character. The ligand orbitals are usually referred to the ligand as origin, e.g., oxygen 2s, 2p or chlorine 3s, 3p. For computational purposes—even the notional ones discussed here—it is more enlightening to refer all functions to the metal as common origin. Standard expressions²² are available to expand a ligand-centered function as a superposition of metal-centered s, p, d, f, ... functions. The expansion coefficients depend upon factors like bond length and radial form of the ligand orbitals (and hence upon charge distributions). All in all, the LFOs thus comprise dominant metal d character together with metal s, p, f, ... character functions that mostly originate on the ligands.

The electric-dipole selection rule $\Delta l = \pm 1$ then focuses our attention upon just the p and f character admixtures in the LFOs (“d”). Herein lies the origin of the double set of t parameters. In briefest outline, $P_{t\lambda}$ relates to integrals of the form

$$\begin{aligned} \langle \text{“d}_i\text{”} | e\mathbf{r} | \text{“d}_j\text{”} \rangle &\equiv \langle d_i + c_p p_i | e\mathbf{r} | d_j + c_p p_j \rangle = \langle d_i | e\mathbf{r} | d_j \rangle \rightarrow 0 \\ &+ c_j \langle d_i | e\mathbf{r} | p_j \rangle \} \rightarrow P_t + \dots \quad (8) \\ &+ c_i \langle p_i | e\mathbf{r} | d_j \rangle \} \end{aligned}$$

while $F_{t\lambda}$ relate to integrals like

$$\begin{aligned} \langle \text{“d}_i\text{”} | e\mathbf{r} | \text{“d}_j\text{”} \rangle &\equiv \langle d_i + a_f f_i | e\mathbf{r} | d_j + a_f f_j \rangle = \langle d_i | e\mathbf{r} | d_j \rangle \rightarrow 0 \\ &+ a_j \langle d_i | e\mathbf{r} | f_j \rangle \} \rightarrow F_t + \dots \quad (9) \\ &+ a_i \langle f_i | e\mathbf{r} | d_j \rangle \} \end{aligned}$$

where we have artificially separated the p and f character admixtures in the LFOs for heuristic reasons.

Further theory,⁵ which we do not rehearse here, makes qualitative predictions about the dependence of P/F ratios—meaning $P_{t\lambda}/F_{t\lambda}$ —upon metal—ligand bond length, bond polariza-

(22) Sharma, R. R. *Phys. Rev.* **1976**, *A13*, 517.

tion, and bond diffuseness. These predictions appear to be well supported by analyses of some 40 chromophores to date.^{2,4}

Contributions from centrosymmetrically related ligations automatically cancel identically so that the calculated intensities of centric chromophores vanish, as required by Laporte's rule. The model thus far described is our "static" model³ and hence is applicable only to acentric chromophores. Our recently published "dynamic" model⁶ relates to the intensities of centrosymmetric complexes. The model does not contemplate the possibility of strong coupling between electronic and nuclear motions such as characterize a breakdown of the Born–Oppenheimer approximation. That lay behind our choice of the name "dynamic" but we are persuaded that, even with the proviso above, the name "vibronic" is proper.

In this approach, parity mixing within the LFOs—and hence intensity in the "d–d" transitions—is envisaged to arise during the course of *ungerade* molecular vibrations. The vibrations are several orders of magnitude slower than the electronic excitations so the encounter of a light beam with a macroscopic sample of the chromophore may be viewed as the interaction of photons with chromophores in every possible phase of their vibration cycles. Different normal modes are uncorrelated so intensity arising from them will be additive. We therefore develop a theory for a chromophore that is distorted along one normal mode by a fixed amount. Subsequently we recognize the full vibration cycle by integration. Finally we sum intensity contributions from different modes. It was to be expected from the beginning that vibrations with the greater amplitudes will be the better generators of intensity in this way. Intensity may arise from both bending and stretching modes. In outline, our modeling of intensity arising from molecular bends is as follows.

We parameterize the local transition moments of a ligand which is displaced from its equilibrium position in a direction that is determined by the normal mode under consideration. The relevant parameters are just those of the static model above. Those transition moments are then referred to the local equilibrium frame. This is precisely the same reference frame we would employ in the static model and, of course, corresponds to that obtainable from a crystallographic structure analysis. The result of this transformation is one part that is independent of the ligand displacement and one part that, for small displacements at least, is linearly dependent upon the angular displacement sustained in the bend. The displacement-independent parts for centrosymmetrically related ligands cancel when ultimately transformed into the common global frame. Within *gerade* bending vibrations, the corresponding displacement-dependent parts also cancel, as required by Laporte's rule once again. For *ungerade* bends, however, the displacement-dependent parts of transition moments for diametrically opposite ligands add numerically in the global frame and so give rise to intensity. These local transition moments are parameterized with the quantities $L_{t\lambda}^{\alpha}(Q)$ for ligand displacements in direction α within the normal mode (Q).

The completion of the vibronic intensity model proceeds as for the static one: locally parameterized moments are transformed into the global frame and summed, and so on. Instead of the intensity parameter set $L_{t\lambda}$ ($L = P, F; \lambda = \sigma, \pi_x, \pi_y$) for each ligation type, we have the same but for each normal mode. The degree of parameterization is clearly larger and potentially too large to support definitive analysis within the typically limited experimental data base. Some problems of this kind were encountered within the first analyses using the dynamic model. Nevertheless, ambiguities or not, successful accounting for the intensity distributions in the polarized spectra of several tetrahalocopper(II)⁷ and -platinum(II)⁸ chromophores has been

possible. Those successes have encouraged us to pursue the vibronic model one step further. This is the point of departure for the present series of studies.

The full theoretical exposition of the vibronic model defines the vibronic $L_{t\lambda}^{\alpha}(Q)$ parameters in terms of the "underlying" static $L_{t\lambda}$ parameters (of the initially envisaged displaced ligand) and of the root-mean-square (rms) angular displacement suffered by the relevant ligand within the given normal mode:

$$L_{t\lambda}^{\alpha}(Q) = \theta_Q^{\alpha} L_{t\lambda} \quad (10)$$

If these rms ligand displacements are known or can be reasonably estimated, the free parameterization $\{L_{t\lambda}^{\alpha}(Q)\}$ can be replaced with the "static" parameter set $\{L_{t\lambda}\}$. As the latter refer exclusively to electronic features of the underlying metal–ligand bonding, the mechanical aspects of the enabling modes have been "factored out" of the model. Furthermore, modeling of the molecular vibrations by normal coordinate analysis, as described in the following section, simultaneously provides a quantitative account of the temperature dependence of the various rms angular displacements of interest to us. The way is thus open to account for the vibronically sourced "d–d" intensities at different temperatures. This does form part of the present analyses.

The form of (10) allows us to relate the vibronic parameters from one vibration to another, as we have described. It also relates all vibronic parameters to the underlying static ones. This means that not only are analyses of centric and acentric chromophores brought onto the same footing but that near-centric systems, in which intensity derives from both static and vibronic parity mixing, are equally accessible. Such a system is the subject of the following paper.¹⁰

Our treatment of the tangential displacements undergone by ligands within bending vibrations ignores any small variations in bond character throughout the vibration amplitude. We have adopted the view in which a bend is built up of a (continuum of) snapshots of the same chemical molecule but with slightly different geometries. A similar view of stretching vibrations, on the other hand, is not possible. In this case, each "snapshot" throughout the stretching cycle comprises a unique radial geometry. Put otherwise, while it is possible to factorize a bend into a well-treatable, angular factor and a (reasonably) presumed constant radial factor, no such geometric and bonding partitioning may be followed for a stretch. Consequently, a simple relationship like (10) is not available for stretches. Furthermore, because of the different dependence⁵ of $F_{t\lambda}$ and $P_{t\lambda}$ static parameters upon bond length, it is not expected that different stretches will be characterized by the same $F_{t\lambda}/P_{t\lambda}$ ratio for each other or for the (putative or actual) static contribution to intensity. In short, inclusion of stretching vibrations into our vibronic analysis must necessarily be profligate with parameters. We present arguments below to justify their neglect in the present systems.

As mentioned above, our vibronic model takes no account of any breakdown in the Born–Oppenheimer approximation such as would arise under circumstances of significant dynamic Jahn–Teller coupling. The present chromophores seem unlikely to be candidates for such coupling; their D_{2h} (or lower) molecular symmetries, which beget no spatial degeneracies, exist at least by dint of the CuCl_2X_2 coordination.

In principle, a second matter of concern for the applicability of our model to real systems arises when the nuclear motions become significantly anharmonic. Descriptions of the molecular dynamics in terms of the normal modes afforded by the normal coordinate analysis described in the following section become increasingly unsatisfactory with increasing anharmonicity. Hav-

ing argued for the reasonable neglect of dynamic Jahn–Teller effects, we similarly doubt the existence of large ground state anharmonicity from that source. Further, our analyses are based upon electronic spectra measured at low enough temperatures hopefully to render any other anharmonicity negligibly small. The subsequent, successful use^{11–13} of the coth rule, whose theoretical²³ applicability rests with the harmonic assumption in the ground state, suggests that our approximations are satisfactory enough.

McDonald and Hitchman^{11–13} have fitted the temperature dependencies of several electronic spectra of the present chromophores to the coth rule, concluding generally that intensity is mainly generated by the low-frequency (bending) modes. This lies behind our neglect of stretches in the present vibronic analyses. Further, insofar that (predominantly) stretching modes may be ignored in these analyses, so also may any stretch components within predominantly bending modes; conversely, if the one is not to be neglected, neither is the other.

Normal Coordinate Analyses. Vibrational spectra may be analyzed quantitatively using Wilson's GF-matrix method.^{24,25} When expressed in terms of internal coordinates, the vibrational problem reduces to the familiar secular equation

$$\mathbf{GFL} = \Lambda \mathbf{L} \quad (11)$$

where \mathbf{F} and \mathbf{G} are respectively the potential and inverse kinetic energy matrices, Λ is a diagonal matrix whose elements are proportional to the squares of the harmonic vibrational frequencies $\{\nu\}$, and \mathbf{L} contains the eigenvectors. These latter relate the internal coordinate vector \mathbf{s} to the normal coordinate vector \mathbf{Q} such that $\mathbf{s} = \mathbf{LQ}$. In the harmonic approximation, the Cartesian displacement coordinates $\{x\}$ are linearly related to the internal coordinates by the matrix equation $\mathbf{s} = \mathbf{Bx}$. The elements of the \mathbf{B} matrix are determined by the molecular geometry. It follows that

$$\mathbf{x} = \mathbf{B}^{-1}\mathbf{LQ} \quad \text{or} \quad \mathbf{x} = \mathbf{L}_x\mathbf{Q} \quad \text{where} \quad \mathbf{L}_x = \mathbf{B}^{-1}\mathbf{L} \quad (12)$$

The atomic displacements for a unit displacement of the normal coordinate Q_i are given by the i th column of the \mathbf{L}_x matrix.

The rms amplitude of the normal coordinate Q_i at temperature T is given²⁶ by its expectation value

$$\langle Q_i \rangle^2 = \frac{h}{8\pi^2 c \nu_i} \coth\left(\frac{Lc\nu_i}{2kT}\right) \quad (13)$$

for each normal coordinate. The rms displacements at any temperature may be calculated if the secular equation can be solved and the harmonic approximation is valid.

We have written a new normal coordinate analysis program in order to obtain this information from the vibrational spectra of transition metal complexes. The program has been extensively checked by repeating numerous published analyses, including the IUPAC test-data package.²⁷ All calculations used symmetry and/or internal coordinate basis sets within the modified general valence force field. A facility for refinement by least-squares fitting is included in the program.²⁸

Table 8. Observed Vibrational Frequencies (cm^{-1}) for CuCl_2X_2 Chromophores^a

mode	symmetry ^b	PDMP	2,3-LUT	2,6-LUT	DIAQ	4-PICNO
ν_1	a_g	125	142	139	444	413
ν_2	a_g	246	251	245	252	292
ν_3	b_{1g}	145	153	158	246 ^c	229
ν_4	b_{1u}	71	73	68	167	15
ν_5	b_{1u}	78	90	94	71 ^d	70, 100, 130 ^e
ν_6	b_{2u}	316	321	316	333	332
ν_7	b_{2u}	142	150	152	277	203
ν_8	b_{3u}	240	268	241	445	435
ν_9	b_{3u}	151	150	155	182	173

^a By use of the parameter values in Table 9, all calculated frequencies agree with these to within $\pm 1 \text{ cm}^{-1}$. ^b In D_{2h} symmetry. ^c Taken from spectrum^{29,30} of $\text{K}_2\text{CuCl}_4 \cdot 2\text{H}_2\text{O}$. ^d Very weak feature; assigned on the basis of the normal coordinate analysis. ^e Uncertain frequency; three trial values considered—see text.

The infrared (IR) and Raman spectra of each of the copper(II) complexes have been recorded by Hitchman and McDonald.^{11–13} These authors also assigned the spectra by careful reference to related systems, especially the bromo analogues, and by using normal coordinate calculations. We have followed their assignments, and their force constants have been used unchanged for DIAQ and as starting values for the other systems. Observed frequencies and assignments are listed in Table 8.

For the normal coordinate analyses, the true molecular geometries have been employed. However, in view of the limited vibrational data base, only the CuCl_2X_2 chromophores have been studied; that is, ligands were dealt with as *pseudo* monatomic entities. We have made the approximation that the internal vibrations of the various ligands, being of high frequency, are little coupled with those of the CuCl_2X_2 chromophores. Figure 4 defines the internal coordinates used in these analyses and shows normal modes and symmetries (in the D_{2h} approximation) for the *ungerade* bends. Directions, but not relative amplitudes, of displacements are shown. The refined force constants are listed in Table 9; they reproduce all the observed frequencies of Table 8 to within 1 cm^{-1} .

The low-energy out-of-plane b_{1u} mode (ν_5) is not observed in the IR spectrum of 4-PICNO. In the DIAQ system, this mode is assigned by Hitchman and McDonald^{11,13} to a weak feature at 71 cm^{-1} on the basis of their calculations. Initially the same frequency was used in the analysis of 4-PICNO. The low energy of this mode is very important in determining the temperature dependence of the intensity of the electronic spectrum of this chromophore. As described below, this frequency did not yield a very good description of the high-temperature spectrum. To study this, calculations were also completed using ν_5 frequencies of 100 and 130 cm^{-1} .

As discussed above, only *ungerade* bending modes have been included as effective intensity generators within our vibronic analyses. There are four such modes in the present systems. Two are out-of-plane bends of b_{1u} symmetry. Of these, the mode labeled ν_5 sends the system toward a tetrahedron. The other, labeled ν_4 , involves an "umbrella" type motion. These modes strongly resemble the b_{2u} and a_{2u} modes, respectively, of the square planar D_{4h} geometry. The magnitudes of the various ligand displacements are found to be quantitatively similar in each system. Due to the relative softness, or low energy, of these modes, the displacements increase markedly with temperature, as dictated by eq 13.

(23) Lohr, L. L., Jr. *J. Chem. Phys.* **1969**, *50*, 4596.

(24) Wilson, E. B., Jr.; Decius, J. C.; Cross, P. C. *Molecular Vibrations*; McGraw-Hill: New York, 1955.

(25) Califano, S. *Vibrational States*; Wiley: New York, 1976.

(26) Cyvin, S. J. *Molecular Vibrations and Mean Square Amplitudes*; Elsevier: Amsterdam, 1968.

(27) Tasumi, M.; Nakata, M.; Durig, J. R.; Jones, R. N.; Schutte, C. J. H.; Zerbi, G. *Pure Appl. Chem.* **1985**, *57*, 121.

(28) Bridgeman, A. J.; Gerloch, M. VANAL, a FORTRAN computer program, 1993.

(29) Adams, D. M.; Newton, D. C. *J. Chem. Soc. A* **1971**, 3507.

(30) Bansal, M. L.; Sahni, V. C.; Roy, A. P. *J. Phys. Chem. Solids* **1979**, *40*, 109.

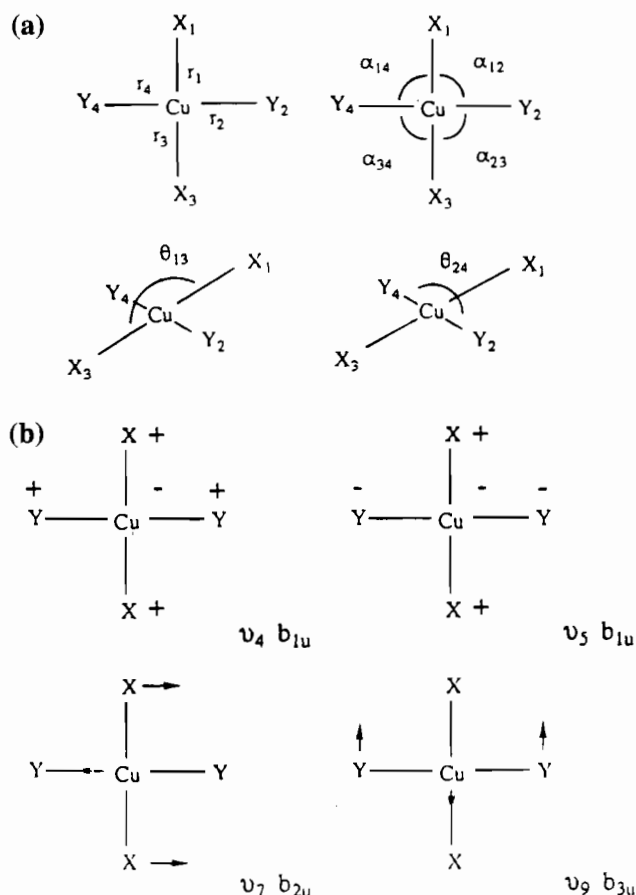


Figure 4. (a) Internal coordinates used for normal coordinate analysis. (b) Normal *ungerade* bending modes in MX₂Y₂ species.

The other two *ungerade* bends involve in-plane motion and are of b_{3u} and b_{2u} symmetry in the *D*_{2h} approximation. They may be derived from the e_u mode in square-planar systems. Each involves essentially only movement of *trans*-related ligand pairs. Mixing of these modes due to the lower symmetry of the real molecules is reasonably important and is not neglected in the present vibronic analyses. Such mixing is a factor in reducing the utility of the *D*_{2h} selection rules in the assignment of the electronic spectra of these species.

The displacements associated with the b_{2u} and b_{3u} modes are qualitatively similar for the five systems. This may be somewhat surprising for the DIAQ complex because of the low mass of the water ligands. However, the hydrogen bonding to two phosphine oxide molecules in the lattice is probably relevant. The effect of hydrogen bonding on the vibrations of the coordinated water has been investigated by McDonald.¹³ Although the displacements of the b_{2u} and b_{3u} modes are comparable to those of the out-of-plane bends at low temperatures, their higher energy leads to a slower increase in the amplitude with temperature.

The rms displacements and hence angular displacements of ligands relative to the central metal atom have been calculated for each of those four modes, for each chromophore, and at each temperature of interest. These relate to the vibrations from the true crystallographic geometries. In our vibronic intensity model, no reduction in parameterization or cost is gained by approximating to any ideal geometry. On the other hand, as discussed already, our descriptions of the force fields in the present chromophores are approximate because of the replacement of the real multiatomic N or O ligands by appropriate *pseudoatoms*. We detail in the Appendix, fits to observed electronic intensity distributions corresponding to 20% devia-

tions of each donor atom displacement from those yielded by the above NCA analyses. While such fits are less good than those presented in full below, they are not markedly so. We conclude that the present force-field descriptions are satisfactory for our vibronic analyses.

Intensity Analyses. For each centric chromophore, we have considered “d–d” intensity to arise through vibronic parity mixing within the course of each of the four normal bending modes described in the preceding section. All $L_{t\lambda}(Q)$ parameters are related to underlying “static”-type $L_{t\lambda}$ parameters *via* the displacements computed within the foregoing normal coordinate vibrational analyses. The CLF intensity parameter set then comprises the following: $F^{P}t_{\sigma}(\text{Cl})$, $F^{P}t_{\pi}(\text{Cl})$, and $F^{P}t_{\sigma}(\text{O or N})$ for each of the five chromophores, together with $F^{P}t_{\pi\perp}(\text{N})$ for the CuCl₂N₂ species, together with $F^{P}t_{\pi\perp}(\text{O})$ for the CuCl₂O₂ species, together with $F^{P}t_{\pi\perp}(\text{N})$ for the CuCl₂N₂ species, $F^{P}t_{\pi}(\text{O})$ for 4-PICNO, or $F^{P}t_{\pi\perp}(\text{O})$ for DIAQ, where \perp is perpendicular to the CuCl₂O₂ coordination plane. All other $L_{t\lambda}$ parameters were held at zero. Each analysis thus considers eight $L_{t\lambda}$ parameters. However, as only relative intensities are accessible within our model, one parameter is held fixed, so leaving seven degrees of freedom.

The experimental data base derives from Gaussian deconvolution of the published spectra of McDonald and Hitchman.^{11,13} Three transitions are resolvable for each of the CuCl₂O₂ systems. Four such are available for the CuCl₂N₂ species, except for one polarization of PDMP for which only three bands may be deconvoluted. Details of bands and polarizations are summarized in Table 10. Bands are labeled by frequency range in Tables 4 and 10. Complete sets of spectral traces, each of which has been recorded at several temperatures over a wide temperature range, are to be found in refs 11–13; we abstract a typical polarization at several temperatures in Figure 5 to facilitate discussions below.

The initial, and most thorough, analytical procedures were concerned to reproduce the lowest temperature experimental data (10 K in each case) *directly*. By this is meant that comparison between observed and calculated intensity distributions are made with reference to the experimental, *crystal* polarization (as listed in Table 10) rather than to derived molecular frames. After preliminary calculations, it was found possible to relate all t parameter values to $t_{\sigma}(\text{Cl})$. Except for 4-PICNO, all seven parameters were varied independently and together. Fitting regions were identified at first by variation of parameters, two or three at a time. For 4-PICNO, $t_{\sigma}(\text{Cl})$ was found to be very small and was subsequently held at zero, so reducing the degree of parameterization to six (equal to the number of independent observables). A single region of parameter space was found to yield good fits for each of the five chromophores. The optimal parameters reported in Table 11 were obtained in each case by the least-squares facilities⁹ in CAMMAG4, starting from within these “unique” parameter regions. The values shown there have been scaled to yield the observed absolute intensities. A number of checks have shown these calculated intensities to vary insignificantly with the spin–orbit coupling coefficient, for $\zeta = 700 \pm 200 \text{ cm}^{-1}$. The quality of reproduction of all experimental intensities is illustrated by the histograms in Figure 6. Apart from the problems encountered with the intensity analyses of the CuCl₂N₂ chromophores with the first-chosen energy assignment, all intensity analyses proceeded remarkably smoothly.

In general we find that all four bends contribute significantly and, conversely, that no one bend is dominant. Equally general is that the relative contributions of the different bends is significantly different for $\zeta = 700 \text{ cm}^{-1}$ than for $\zeta = 0$. This

Table 9. Optimal Force Constants (mdyn Å⁻¹)^a

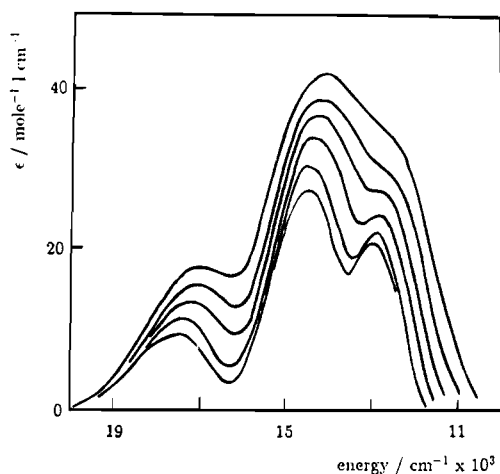
constants ^b	PDMP	2,3-LUT	2,6-LUT	DIAQ	4-PICNO ^c		
					a	b	c
$f_t(X)$	1.524	1.421	1.261	1.841	2.437		
$f_t(Y)$	1.133	1.159	1.129	1.207	1.394		
$f_{rr}(XY)$	0.001	0.001	0.001	0.016	0.012		
$f_{rr}(X)$	0.060	-0.150	-0.049	0.251	0.577		
$f_{rr}(Y)$	0.131	0.157	0.127	0.127	0.387		
$f_{\alpha} - f_{\alpha'}$	0.263	0.254	0.260	0.299	0.231		
$f_{\alpha\alpha} - f_{\alpha\alpha'}$	0.032	0.050	0.027	0.050	0.054		
$f_{\alpha\alpha} - f_{\alpha\alpha'}(X)$	0.294	0.298	0.277	0.280	0.159		
$f_{\alpha\alpha} - f_{\alpha\alpha'}(Y)$	0.084	0.070	0.084	0.112	0.072		
$f_{\theta}(X)$	0.072	0.065	0.057	0.056	0.064	0.087	0.110
$f_{\theta}(Y)$	0.048	0.055	0.055	0.059	0.059	0.086	0.131
$f_{\theta\theta}(XY)$	-0.037	-0.032	-0.026	0.021	0.015	-0.010	-0.044

^a Cross terms represented by *cis* (f_{s1s2}) and *trans* (f_{s1s2}) interaction force constants.²⁵ ^b X = O, N; Y = Cl. ^c a yields $\nu_5 = 70$ cm⁻¹; b yields $\nu_5 = 100$ cm⁻¹; c yields $\nu_5 = 130$ cm⁻¹.

Table 10. Experimental Polarizations for CuCl₂X₂ Electronic Spectra

chromophore	abbrev ^a	polarization direction
PDMP	POL 1	[100] direction in (001) face
	POL 2	[010] direction in (001) face
2,3-LUT	POL 1	76° to [001] direction in (010) face
	POL 2	-14° to [001] direction in (010) face
2,6-LUT	POL 1	55° to [100] direction in (001) face
	POL 2	-35° to [100] direction in (001) face
4-PICNO	POL 1	35° to [100] direction in (011) face
	POL 2	-55° to [100] direction in (011) face
DIAQ	POL 1	[001] direction in (100) face
	POL 2	[010] direction in (100) face
	POL 3	[102] direction in (200) face.

^a Appearing as labels in Figure 6.

**Figure 5.** Observed absorbance spectra for 4-PICNO in polarization POL 2 (see Table 10). The increasing spectral traces are for temperatures 10, 50, 100, 150, 200 and 250 K, respectively.

clearly indicates that care must be used when assigning vibronically sourced “d–d” spectra using selection rules built without recognition of the role of spin–orbit coupling.

Finally we address the temperature variations of the “d–d” spectral intensities. As described in the preceding section, our normal coordinate analyses have furnished the magnitudes of all ligand displacements as functions of temperature. In principle, therefore, we might contemplate carrying out independent intensity analyses, as above, for data obtained at each experimental temperature. However, as the typical spectra in Figure 3 show, Gaussian resolution of the observed spectral traces becomes progressively more uncertain for data at increasing temperatures. Resolution is moderately acceptable up to ca. 100 K (or up to 150 K in a couple of cases) but essentially

Table 11. Optimal CLF Intensity Parameters ($D \times 10^{-2}$) for CuCl₂X₂ Chromophores

	PDMP	2,3-LUT	2,6-LUT	DIAQ	4-PICNO
$^p f_{t\sigma}(Cl)$	87	45	33	126	166
$^f f_{t\sigma}(Cl)$	24	38	30	1	0
$^p f_{t\pi}(Cl)$	5	3	2	57	118
$^f f_{t\pi}(Cl)$	5	3	2	19	35
$^p f_{t\sigma}(X)$	3	100	72	68	158
$^f f_{t\sigma}(X)$	87	32	31	116	10
$^p f_{t\pi\parallel}(X)$	0 ^a	0 ^a	0 ^a	0 ^a	48
$^f f_{t\pi\parallel}(X)$	0 ^a	0 ^a	0 ^a	0 ^a	0
$^p f_{t\pi\perp}(X)$	25	11	0	24	48 ^b
$^f f_{t\pi\perp}(X)$	21	9	2	125	0 ^b

^a Fixed. ^b || set equal to \perp .

impossible at higher temperatures. We have met these problems in two ways. Where acceptable resolution of spectral bands has been possible, we have calculated intensity distributions using the optimal $^L t_{\lambda}$ parameter values obtained from the 10 K analyses together with appropriate ligand displacements at each temperature obtained from the vibrational analysis. We find these calculated intensities to compare reasonably well with the experimental values. Unacceptable reproduction of the experimental band intensities for data obtained above ca. 100 K correlates with the difficulty in performing the corresponding spectral deconvolutions. For the higher temperatures (indeed for all temperatures, for completeness' sake), we have adopted the following tactic. Again using the 10 K $^L t_{\lambda}$ parameter values and vibrationally determined ligand displacements, we have made comparisons of the total “d–d” intensity corresponding to integration over all bands and all experimental polarizations. The quality of agreement between observation and calculation was now found to be comparable to that obtained for the individual (resolved) bands at the lower temperatures. Such was true for all systems except 4-PICNO. As noted in the preceding section, the ν_5 vibration was not observed for this chromophore but taken initially as 70 cm⁻¹ by comparison with ν_5 in DIAQ. We have repeated the 10 K analysis for 4-PICNO with ligand displacements corresponding to ν_5 being 70, 100, and 130 cm⁻¹. Subsequent comparison of the “integrated” spectra (i.e., over all bands and polarizations) for ν_5 taking each of these values is summarized in Figure 7. Satisfactory agreement with the observed temperature dependence of the “d–d” intensities in 4-PICNO is obtained for ν_5 around 100 cm⁻¹.

Discussion

This paper describes the first applications of our complete vibronic model for “d–d” intensities in which prior vibrational analysis allows the separation of mechanical and electronic

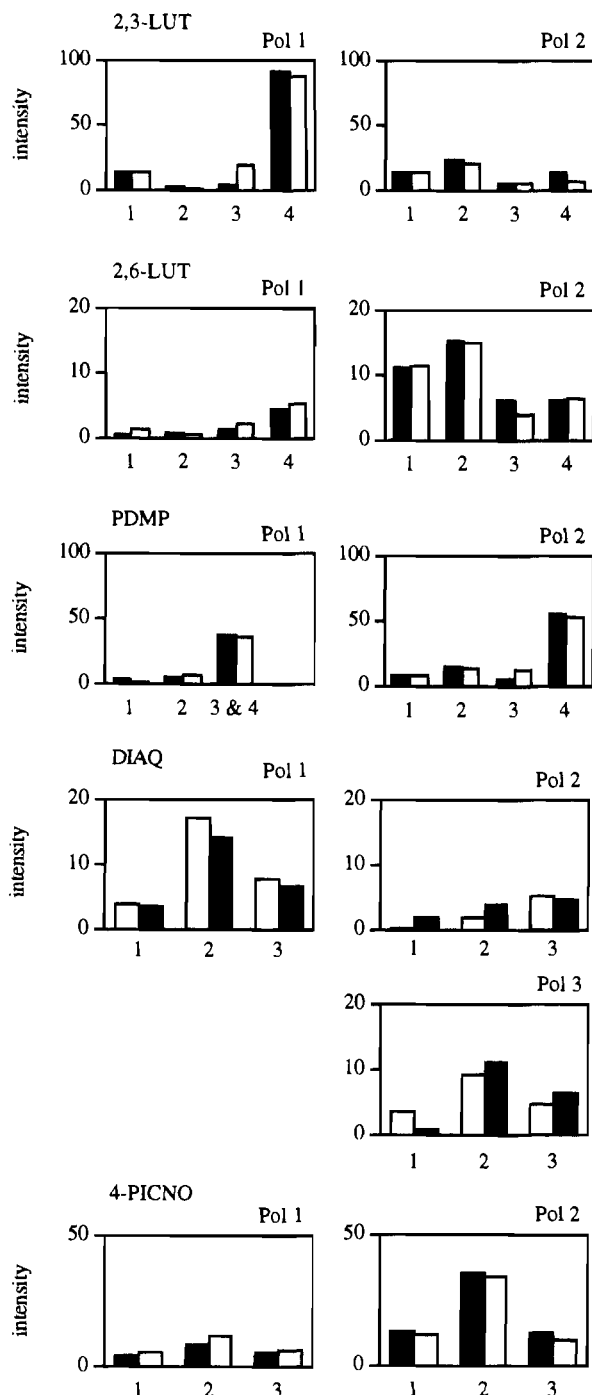


Figure 6. Comparisons between observed intensities and those calculated using the optimal parameter sets of Tables 3, 7 and 11. Bands are labeled in Tables 4 and 6. Polarization directions are identified in Table 10. Observed band areas are shown in solid black. Intensities are plotted in units of $D^2 \text{ cm}^{-1} \times 15$.

information. They have been entirely successful in that observed intensity distributions and their dependences upon temperature have been reproduced quantitatively. All CLF intensity analyses are predicated upon appropriate energy studies. A byproduct of the present intensity work is the resolution of some assignment ambiguities and hence of some uncertainties in these energy analyses. The DIAQ chromophore illustrates a particularly interesting point. We begin with these matters and then move on to consider some very important aspects of the ligand-field parameter values themselves.

Band Assignments. As described under Transition Energies above, fitting the intensity distributions of the CuCl_2N_2 species

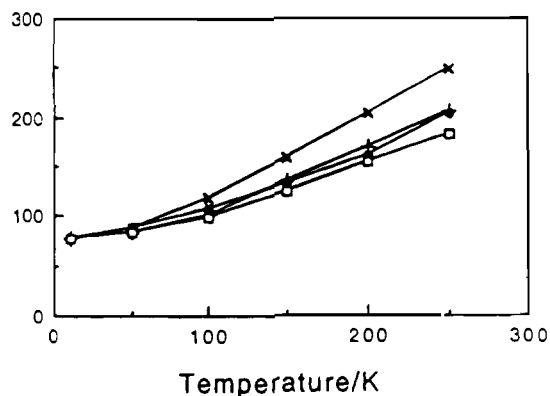


Figure 7. Temperature dependence of the total electronic spectral intensity for 4-PICNO (same units as for Figure 6): obsd (●); $\nu_5 = 70 \text{ cm}^{-1}$ (×); $\nu_5 = 100 \text{ cm}^{-1}$ (+); $\nu_5 = 130 \text{ cm}^{-1}$ (□).

has unambiguously established the “alternative” band assignment described. Clearly the double study of energies plus intensities has been essential in this case. For 4-PICNO, the intensity analysis has served to confirm the assignments originally proposed by Hitchman and McDonald¹¹ and indeed to confirm the bonding picture underlying eq 2. The situation for the DIAQ chromophore is especially intriguing.

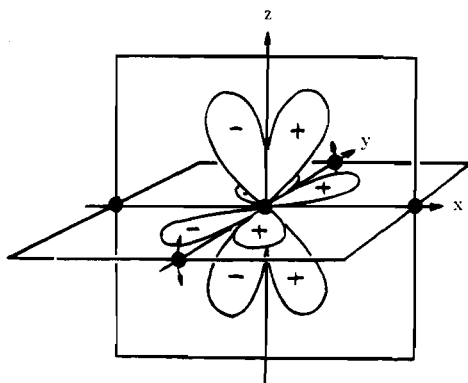
The energy analysis for DIAQ proceeded on the basis of the sort of copper–oxygen bonding that is likely to follow the crystal-determined hydrogen bonding in this system. Both transition energies and subsequent intensity distributions were quantitatively accounted for on this basis despite our ignoring the group theoretically established—and contrary—assignment¹¹ of Hitchman and McDonald. The central issue here is the observed weakness in crystal b polarization (which corresponds very closely to the molecular z polarization) of what our analysis assigns as the $xz \rightarrow x^2 - y^2$ transition. This is formally enabled by a b_{3u} vibration. In the present system, we find it not to be enabled at all by the b_{3u} bend. Thus, Table 12 lists molecular state intensities calculated with the optimal $L_{t\lambda}$ parameters of Table 11 but using the b_{3u} bend *alone*. It shows the $xz \rightarrow x^2 - y^2$ transition in the z polarization to be uniquely extremely weak. This extra “selection rule” obviously underlies our successful accounting for the observed intensity distribution in this complex; at the same time it removes any conflict between Hitchman and McDonald’s work¹¹ and our own. The question remains, however, as to *why* the b_{3u} bend is uniquely ineffective as an intensity generator for this particular transition.

The transition moment $\langle xz|ez|x^2 - y^2 \rangle$ involves electronic displacement in the xz global plane alone. As shown in Figure 4, the b_{3u} bend involves tangential displacements of the chlorine atoms, lying along the global y axis, parallel to z. This ligand motion is ultimately responsible for inducing parity mixing into the d orbital basis and hence for generating spectral intensity. The odd-parity functions admixed into the d that circumvent the orbital selection rule, $\Delta l = \pm 1$, are of p or f type. If p, the chlorine atom displacement admixes p_y into $d_{x^2-y^2}$. However, the resulting $p_y - d_{x^2-y^2}$ hybrid differs from the pure $d_{x^2-y^2}$ function only in spatial regions on either side of the xz plane. The $\langle xz|ez|x^2 - y^2 \rangle$ transition moment is not, therefore, expected to be affected or enabled by this particular parity-mixing process. The same is not true for d–f mixing. Consider, for example, the admixture of $f_{x(y^2-z^2)}$ character into the $d_{x^2-y^2}$ as will be facilitated by the b_{3u} bend. As shown in Figure 8, the f function is concentrated in both xy and xz planes. Changes in the d–f mixing in the xy plane brought about by the displacement of the chlorine atoms are necessarily accompanied by changes in d–f mixing in the xz plane. Accordingly, the $\langle xz|ez|x^2 - y^2 \rangle$

Table 12. DIAQ Molecular State Intensities Calculated with Optimal Parameters of Table 11 but for Contributions from the b_{3u} Bend Alone, and for 10 K

band	energy/cm ⁻¹	calculated intensity/D ² cm ⁻¹			orientation with respect to global frame ^a								
		min	med	max	min			med			max		
1	13 329	253×10^{-5}	162×10^{-3}	391×10^{-3}	90	90	0	120	30	90	30	60	90
2	14 831	425×10^{-3}	763×10^{-3}	428×10^{-2}	90	90	0	97	7	90	7	83	90
3	15 469	560×10^{-1}	145×10^{-3}	283×10^{-2}	90	90	0	24	114	90	66	24	90
4	17 915	853×10^{-1}	366×10^{-3}	375×10^{-1}	90	90	0	88	2	90	178	88	90

^a x is approximately \parallel Cu-O, y is \parallel Cu-Cl, and z is \perp coordination plane.

**Figure 8.** The $f_{x(y^2-z^2)}$ function in relation to the global molecular frame for DIAQ.

transition moment is expected to be sensitive to the b_{3u} bend via the d-f parity mixing but not, as we have seen, by the d-p mixing. Now the optimal parameter values of Table 11 that were used to construct Table 12 involve a total dominance of 1T_g over 3T_g and we do indeed observe a near-vanishing value for the $xz \rightarrow x^2 - y^2$ intensity. Table 13 lists the same molecular state intensities as Table 12, again for the b_{3u} bend only, but with the values of $^1T_g(\text{Cl})$ and $^3T_g(\text{Cl})$ reversed. Now we observe, as just predicted, a significant value for the $\langle xz|ez|x^2 - y^2 \rangle$ transition moment.

Overall, then, the origins of the extra "selection rule" in this system lie in the inability of the b_{3u} bend to affect the parity mixing of the orbitals in the xz plane via d-p mixing processes. Even this rule will be violated a little if the amplitude of the bend were sufficient to induce some p_x - $d_{x^2-y^2}$ mixing. This last remark is supported further by noting that the b_{3u} stretch—involving *ungerade* changes in the Cu-O bond lengths—is an effective intensity generator for the $xz \rightarrow x^2 - y^2$ transition in z polarization for both d-p and d-f mechanisms. In short, the weakness of the $xz \rightarrow x^2 - y^2$ transition in z polarization depends upon the dominance of p character in the admixed functions over f (both deriving predominantly from the ligands) in this case, upon the ligand displacements being dominated by bending rather than stretching, and, to a small extent, upon the bending amplitudes being dominated by tangential displacements parallel to x with only small components parallel to y .

CLF Parameter Values. As explained in the Transition Energies section, it has been impossible to resolve $e_\sigma(\text{Cl})$ from $e_\sigma(\text{X})$, X = N or O, in any of the present planar species. Analysis furnishes their average, \bar{e}_σ . That apart, the analyses for the CuCl_2N_2 species were able to establish unambiguous values for all e_λ variables \bar{e}_σ , $e_\sigma(\text{void})$, and appropriate e_π parameters, and of the ligand-field trace^{31,32} Σ defined as the sum of $e_\sigma + e_{\pi_x} + e_{\pi_y}$ for all ligations, including coordination

voids. Partly because of less good spectral resolution and partly because of the more complex bonding (misdirected valency), the energy analyses for the CuCl_2O_2 species are less exact. However, the employment of reasonable assumptions has provided for values of \bar{e}_σ , $e_\sigma(\text{void})$ and Σ in which we can place considerable confidence.

First we note that Σ values for 4-PICNO and DIAQ are ca. 24 000 and 22 000 cm^{-1} , values that are in line with trace values determined for scores of other metal(II) complexes of various coordination numbers and geometries for many types of ligand. On the other hand, the trace values for the present CuCl_2N_2 species—ca. 28 000, 27 000, and 30 300 cm^{-1} for 2,3-LUT, 2,6-LUT, and PDMP, respectively—are all significantly larger than what we have previously come to regard as "normal". These higher Σ values are not without precedent, however, figures of ca. 28 000 cm^{-1} having been observed³³ for $[\text{Cu}(\text{imidazole})_6]^{2+}$ and $\text{Cu}(\text{imidazole})_4(\text{NO}_3)_2$.

In parallel with this grouping of trace values, we next note the mean, in-plane \bar{e}_σ values found for the present chromophores. For 4-PICNO and DIAQ, \bar{e}_σ is 5700 and 5450 cm^{-1} , respectively; for PDMP, 2,3-LUT, and 2,6-LUT, it is 6550, 6550, and 6350 cm^{-1} , respectively. The following three arguments suggest that these figures reflect an underlying characteristic of the ligand-field strength of these nitrogen donors being greater than that of the oxygen donors. (a) If $e_\sigma(\text{Cl})$ is the same in all five compounds, $e_\sigma(\text{N}) > e_\sigma(\text{O})$; (b) if $e_\sigma(\text{Cl})$ is the same as in planar CuCl_4^{2-} species (5300 cm^{-1}), then $e_\sigma(\text{N}) \approx 7700 \text{ cm}^{-1}$; (c) if $e_\sigma(\text{Cl})$ is less in conjunction with higher $e_\sigma(\text{X})$ values, reflecting the operation of the electroneutrality principle, the consequent difference between $e_\sigma(\text{O})$ and $e_\sigma(\text{N})$ is even greater than just estimated.

Values for $e_\sigma(\text{void})$ similarly group according to oxygen or nitrogen donor ligands in these compounds: for CuCl_2O_2 , $e_\sigma(\text{void}) \approx -3100 \text{ cm}^{-1}$, and for CuCl_2N_2 , $e_\sigma(\text{void}) \approx -2650 \text{ cm}^{-1}$. For the present analyses, we might be a little less certain of these results for the oxygen species than for the nitrogen, as discussed above and earlier. Nevertheless, the value of $e_\sigma(\text{void})$ for the "normal"-type complexes—meaning "normal" Σ value—is quite typical. The less-than-normal value of $e_\sigma(\text{void})$ for these CuCl_2N_2 species is well established here. Altogether it is clear that the CuCl_2N_2 species are indeed characterized by an "atypical" Σ value, which is in turn determined by the large $e_\sigma(\text{N})$ values and, to a lesser extent, by the numerically smaller $e_\sigma(\text{void})$ value. We return to $e_\sigma(\text{void})$ later. For the moment we focus upon the large $e_\sigma(\text{N})$ values; this turns out to provide important insight into the chemical significance of CLF e_λ values in general.

The values of $e_\sigma(\text{N})$ in these species are not only large compared with $e_\sigma(\text{O})$ or $e_\sigma(\text{Cl})$. They are large too when compared with corresponding values for amine ligands. Our general experience is that metal-amine or metal-ammine

(31) Deeth, R. J.; Gerloch, M. *Inorg. Chem.* **1985**, *24*, 1154.(32) Woolley, R. G. *Chem. Phys. Lett.* **1985**, *118*, 207.

(33) R. J. Deeth, Ph.D. Thesis, University of Cambridge, Cambridge, UK, 1985.

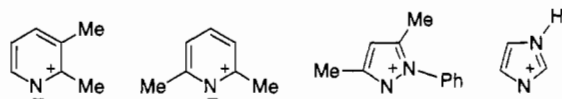
Table 13. DIAQ Molecular State Intensities Calculated with Optimal Parameters of Table 11, Except That the Values of $P_{t\sigma}(\text{Cl})$ and $F_{t\sigma}(\text{Cl})$ Are Reversed, for the b_{3u} Bend Alone, and at 10 K

band	energy/cm ⁻¹	calculated intensity/D ² cm ⁻¹			orientation with respect to global frame ^a								
		min	med	max	min			med			max		
1	13 329	180 × 10 ⁻²	967 × 10 ⁻²	115 × 10 ⁰	169	101	90	102	12	90	90	90	0
2	14 831	104 × 10 ⁻¹	145 × 10 ⁻¹	591 × 10 ⁻¹	171	99	90	90	90	0	99	9	90
3	15 469	105 × 10 ⁻²	331 × 10 ⁻²	134 × 10 ⁰	90	90	0	172	98	90	98	8	90
4	17 915	139 × 10 ⁻²	367 × 10 ⁻²	101 × 10 ⁰	98	8	90	90	90	0	8	82	90

^a Defined in Table 12.

ligations are characterized by $e_{\sigma}(\text{N})$ values that are only somewhat larger than those for metal–oxygen donors. Then, in particular, the $e_{\sigma}(\text{N})$ values for equatorial Cu–en (en = ethylenediamine) bonds in $\text{Cu}(\text{en})_2(\text{BF}_4)_2$ are 6500 cm⁻¹, and for equatorial Cu–NH₃ linkages in various *trans*-Cu(NH₃)₄X₂ species range¹⁷ 5700–6400 cm⁻¹. At this point, comparisons between nitrogen ligands and those with other donor atoms may be less useful as too many factors change at the same time. On the other hand we have here an undiscardable fact that $e_{\sigma}(\text{N})$ values for the nitrogen heterocycles with copper(II) are much larger than $e_{\sigma}(\text{N})$ values for en or ammonia. In short, the ligand-field strength (as e_{σ}) of these heterocyclic imines is considerably greater than that of amines. General chemical experience, on the other hand, suggests that the amines are the better donors toward transition metals; in some support of this, we note the $\text{p}K_{\text{a}}$ values³⁴ for pyridine, pyrazole, and methylamine are 5.2, 2.5, and 10.6, respectively. Furthermore, this generalization is in accord with our characterizing amines as formal sp³ donors but imines as sp².

We propose that the key to an understanding of the reversed trend for $e_{\sigma}(\text{N})$ values and σ donor strength lies in the polarity of the heterocycles. Polarized canonical forms of these ligands,



illuminate the tendency to accumulate negative charge on the (donor) nitrogen atom. We expect the σ donor ability of these heterocycles to be good—though not as good as for amines—even without this “extra” polarization. Hence we ascribe the large e_{σ} values for these cyclic imines as reflecting the conjunction of good base strength with negative charge on the donor atom.³⁵ As ligand-field parameters reflect charge distributions in transition metal complexes *as formed* (that is, after complexation of the metal), this view includes the idea that polarity of the ligand is not significantly diminished by bonding to the metal—possibly the reverse. A qualitatively similar polarity in the O–H bonds of DIAQ or in the N–O bonds of 4-PICNO is to be expected. The smaller values of

$e_{\sigma}(\text{O})$ relative to $e_{\sigma}(\text{N})$ in the present systems are then to be ascribed to an intrinsically poorer σ base strength in the oxygen donor ligands. Certainly one observes very poor donor ability in oxygen donor ligands in which O^{δ-}···X^{δ+} polarity is likely to be small, e.g., ClO₄⁻, CO₃²⁻, etc.

Finally, we consider briefly the values of $e_{\sigma}(\text{void})$ that are lower for the CuCl₂N₂ species than the CuCl₂O₂. We view the salient difference between these systems in terms of a greater M–N covalency than M–O. Increasing covalency in the M–L bonds increases the metal character in the bonding orbitals but decreases metal character in the antibonding. Now $e_{\sigma}(\text{void})$ is concerned with the “sum” of the locally in-plane antibonding orbitals, and so increasing covalency in the M–L bonds is expected to decrease the magnitude $e_{\sigma}(\text{void})$. At the same time, increasing M–L covalency will raise the energy of this antibonding orbital, again reducing the magnitude of $e_{\sigma}(\text{void})$. Taken together, increasing covalency in the coordination plane might be expected³⁶ to be associated with a decreasing magnitude in $e_{\sigma}(\text{void})$ and, hence, with an increasing trace, Σ .

Consider now the intensity parameter values established in the present set of five CuCl₂X₂ chromophores. The $\{t_{\lambda}\}$ in Table 11 have been presented on the same scale for ease of comparison. However, some care must be taken when comparing values for different systems, for the absolute experimental absorbances upon which they depend are ultimately determined by difficult measurements of crystal thickness. Comparisons within any one chromophore, on the other hand, especially in relation to P/F ratios should be more reliable. We begin with the three CuCl₂N₂ compounds.

All values for the Lt_{λ} parameters of 2,3-LUT are closely similar to the corresponding ones of 2,6-LUT. In view of the rather different appearance of the experimental spectra of these systems (for reasons of polarization directions and experimental crystal planes), it is gratifying to see the chemical similarity of these compounds reflected in this way. Next note that the P/F ratio for $t_{\sigma}(\text{N})$ —meaning $P_{t\sigma}(\text{N})/F_{t\sigma}(\text{N})$ —in the LUT species is ca. 3 but ca. 1/30 for PDMP. As noted above, the $\text{p}K_{\text{a}}$ values for pyridine and pyrazole are 5.2 and 2.5, respectively. A less good donor function for the pyrazole ligand would be expected to be reflected in a lower P/F ratio. At the same time we expect a somewhat greater polarity on the pyrazole ligand than the pyridine (or lutidenes, here) so that their similar e_{σ} values probably reflect, in essence, a compensation of poorer donor ability in the former ligand by a larger “ionic” contribution to the M–L bonding. The $t_{\pi}(\text{N})$ parameter values are all small. In part this can be associated directly with the modest values for $e_{\pi}(\text{N})$, but experience^{2,4} with t parameters so far suggests that t_{π}/t_{σ} ratios tend to be greater than e_{π}/e_{σ} ; theoretically⁵ that is to

(34) R. O. C. Norman *Principles of Organic Synthesis*; Chapman & Hall: London, 1968.

(35) The theory^{1,18} of the cellular ligand-field model ascribes the magnitude of CLF parameters to so-called “static” and “dynamic” parts: $e_{\lambda} \approx \langle d_{\lambda} | \mathcal{H}^{(1)} | d_{\lambda} \rangle + \langle d_{\lambda} | \sum (\mathcal{H}^{(1)} | \chi_{\lambda} \rangle \langle \chi_{\lambda} | \mathcal{H}^{(1)} | \epsilon_{\lambda} - \epsilon_{\lambda} \rangle | d_{\lambda} \rangle$. Note that the adjectives static and dynamic used in connection with the CLF energy parameterization are not to be confused with the static and dynamic CLF intensity models! The effect of superposing an “extra” ionic bonding contribution onto the basic covalent metal–ligand bonding is primarily to increase $\mathcal{H}^{(1)}$, the globally aspherical one-electron Hamiltonian of refs 1 and 18, in regions outside of the overlap charge density. Nevertheless, we expect an increase in both static and dynamic contributions to e_{λ} values in this way.

(36) Some uncertainty in this prediction must be allowed, however, as an increase in M–L covalency will also increase $\mathcal{H}^{(1)}$ of the CLF expression for e_{λ} in the previous footnote and that would lead to an increase in the magnitude of $e_{\sigma}(\text{void})$.

Table 14^a

band	obsd	best fit	$\nu_5 (b_{1u})$		$\nu_4 (b_{1u})$		$\nu_9 (b_{3u})$		$\nu_7 (b_{2u})$	
			+20%	-20%	+20%	-20%	+20%	-20%	+20%	-20%
Pol 1										
1	1.1	2.6	2.4	2.9	2.1	3.1	3.5	1.8	2.3	2.8
2	1.4	0.9	0.9	1.0	0.8	1.1	1.2	0.7	0.9	1.0
3	3.1	4.9	5.3	4.6	5.0	4.8	4.8	5.0	4.5	5.3
4	9.9	11.4	13.0	9.8	11.1	11.7	11.0	11.6	10.4	12.3
Pol 2										
1	24.4	25.0	23.1	26.7	20.9	30.0	25.3	24.7	31.0	19.1
2	33.9	32.9	31.1	34.7	37.7	27.1	32.0	33.7	30.3	35.5
3	13.1	8.5	8.7	8.3	8.7	8.2	8.6	8.4	8.0	9.0
4	13.1	13.8	15.6	12.1	13.6	14.1	13.5	14.1	12.6	15.0

^a To convert intensity to absolute units multiply by $6.74 \text{ D}^2 \text{ cm}^{-1}$.

be expected from the more "outer" nature of the electric dipole operator compared with the ligand-field potential. We suspect that the small $t_{\pi}(\text{N})$ values in the present systems indicate little overlap of ligand π functions with metal d_{π} . The more significant e_{π} values then reflect the presence of local ligand π density without there being much in the way of bonding overlap. Finally, consider the t values for the copper-chlorine ligations in these CuCl_2N_2 species. The ${}^P t_{\sigma}(\text{Cl})/{}^F t_{\sigma}(\text{Cl})$ ratio for PDMP is significantly larger than for the LUT systems. This we consider to reflect a larger $\text{Cl} \rightarrow \text{Cu}$ donation in the PDMP complex than in the LUT species resulting from the poorer donor function of pyrazole relative to the lutidenes together with the operation of the electroneutrality principle at the metal. We comment upon the small ${}^L t_{\pi}(\text{Cl})$ values in the CuCl_2N_2 species later.

Though conscious of the less precise energy analyses for the CuCl_2O_2 species, some features of their t parameterization seem clear. The F/P ratio for the $t_{\sigma}(\text{O})$ parameters is large for DIAQ but small for 4-PICNO. Larger F contributions to intensity tend to be associated with bond orbitals that are more polarized toward the ligand. We argue that hydrogen bonding within the DIAQ lattice tends to polarize the O-H bonds even more than in "free" water, so strongly favoring the large F/P ratio observed in the DIAQ complex. We also note that the F/P ratios for the $t_{\pi}(\text{O})$ parameters tend to follow those of the $t_{\sigma}(\text{O})$ in both DIAQ and 4-PICNO. It seems probable that this simply reflects the "scrambling" between σ and π bonding that we have argued to be present in these species as a result of the various forms of "misdirected valency". We similarly consider the greater values for ${}^L t_{\pi}$ in the CuCl_2O_2 species than for ${}^L t_{\pi}(\text{N})$ in the CuCl_2N_2 to reflect the misdirected nature of the Cu-O bonding in the former. Finally, it is interesting to compare the various $t(\text{Cl})$ parameters within these two series of compounds. The P/F ratios for $t_{\sigma}(\text{Cl})$ are much larger in the CuCl_2O_2 species than in the CuCl_2N_2 ; the absolute ${}^L t_{\pi}(\text{Cl})$ values and their P/F ratios are again larger in the CuCl_2O_2 series than in the CuCl_2N_2 . All this points to the idea that the chlorine ligands act as better σ and π donors in the CuCl_2O_2 compounds. Recognizing the operation of the electroneutrality principle at the central metal, this better chlorine donor function would follow for a less good oxygen donor ability than for the cyclic imines. Once again this highlights our proposal above that the larger values found for $e_{\sigma}(\text{N})$ than $e_{\sigma}(\text{O})$ do not reflect the ligand polarity so much as the intrinsically better σ donor power of the nitrogen ligands.

Conclusions

This study began as an attempt to reproduce experimental "d-d" intensity distributions in these centric, planar, chromophores and to do so in such a way as to "factor out" the mechanical, vibrational parts of the intensity generation from the electronic. It has been totally successful in this regard. For us, the whole point of studies of transition metal spectra—and of other such electronic properties—is to learn something of the electron distribution within the molecules and hence something of the chemical bonding. The present vibronic model has put all our intensity studies on the same footing and hence refocused our attention onto these important chemical matters. A careful investigation of both energy and intensity parameters in these species has established both general and particular views of the chemical significance of ligand-field parameters. Generally, the values of the intensity parameters are found to be consistent with those of the energy analyses. Similarly, ambiguities of assignment for the energy analyses have been resolved by the more complete intensity study. By and large, interpretations of both energy and intensity parameter values fall well into line with previously established practice both at the technical (ligand field) level and at the common sense (chemical bonding) level. The overall chemical significance of ligand-field parameters has been clarified by the present analyses, in particular by the recognition of how ligand "donicity" is but one of the contributors to these parameters. We have developed a view of the bonding in these CuCl_2X_2 species in which a degree of ligand polarity is maintained—or possibly augmented—by complexation, notwithstanding the electroneutrality principle. In effect, it is possible to satisfy the drive for electroneutrality on the metal atom in these species with the available donor lone pairs yet without the simultaneous ubiquitous achievement of electroneutrality on each ligand atom.

Acknowledgment. A.J.B. and S.J.E. acknowledge receipt of SERC studentships.

Appendix

Table 14 illustrates the sensitivity of the calculated vibronic intensity to the angular displacements of the inducing modes. For each mode, in turn, the displacements determined by normal coordinate analysis have been varied by $\pm 20\%$. The results shown are for 2,6-LUT and use the parameter values presented in Table 11. Similar results are obtained for the other systems.